A Synoptic Climatology of Northern Hemisphere, Cold Season Polar and Subtropical Jet Superposition Events

CROIX E. CHRISTENSON, JONATHAN E. MARTIN, AND ZACHARY J. HANDLOS

Department of Atmospheric and Oceanic Sciences, University of Wisconsin–Madison, Madison, Wisconsin

(Manuscript received 1 August 2016, in final form 26 May 2017)

ABSTRACT

Narrow, tropopause-level wind speed maxima known as jet streams or jets are among the most ubiquitous structural characteristics of Earth's atmosphere. Two species, the polar and subtropical jets, can be observed on any given day. The polar jet is tied, via eddy momentum flux convergence associated with extratropical wave development, to the troposphere-deep baroclinicity of the midlatitudes, while the subtropical jet is tied, by angular momentum constraints, to the poleward edge of the tropical Hadley cell. As a consequence of their different origins, the polar and subtropical jets are separated by both latitude and elevation. However, there are times when these two usually separate features become vertically superposed to form a single, intense jet core designated as a jet superposition or superposed jet. An objective method for identifying tropopause-level jets is employed in the construction of 50-yr cold season (November–March) synoptic climatologies of the Northern Hemisphere polar jet, subtropical jet, and jet superpositions. The analysis demonstrates that while superposition events are relatively rare, there are clear geographical maxima. Superpositions are most frequent in the western Pacific from December through February, with a secondary peak in southern North America and along its eastern seaboard. Consistent with expectations, the spatiotemporal maxima in jet superpositions appear to be coincident with maxima in the polar and subtropical jets.

1. Introduction

Narrow, rapidly flowing currents of air located near the tropopause are known as jet streams or jets. These jets, often found nearly girdling the globe while exhibiting large meridional meanders, are among the most ubiquitous structural characteristics of Earth's atmosphere and are known to play a substantial role in the production of sensible weather in the midlatitudes. As the primary phenomena at the interface between synoptic-scale weather systems and the large-scale circulation, upper-tropospheric jets are particularly important elements of the climate system. Prior observational work has identified three major jet features: the subtropical jet, the polar jet, and the Arctic jet.

The subtropical jet is located at the poleward edge of the Hadley cell (~30° latitude) in the tropical–subtropical upper troposphere (~200 hPa) (Loewe and Radok 1950; Yeh 1950; Koteswaram 1953; Mohri 1953; Koteswaram and Parthasarathy 1954; Sutcliffe and Bannon 1954; Defant and Taba 1957; Krishnamurti 1961; Riehl 1962) and is driven by angular momentum transport forced by differential heating in the equatorial zone. The polar jet sits atop the baroclinicity of the midlatitudes (usually poleward of 30° latitude) and has its speed maxima closer to 300 hPa (e.g., Namias and Clapp 1949; Newton 1954; Palmén and Newton 1969; Keyser and Shapiro 1986; Shapiro and Keyser 1990).

Namias and Clapp (1949) first discussed the polar jet from the perspective of confluence, which drives horizontal frontogenesis. The subsequent concept of the eddy-driven jet is an elaboration of this original insight, suggesting that the polar jet results from the convergence of eddy momentum flux associated with developing waves in a region of enhanced midlatitude baroclinicity (Held 1975; Rhines 1975; McWilliams and Chow 1981; Panetta 1993). Though often identified by a lower-tropospheric westerly wind maximum (Lorenz and Hartmann 2003), the polar jet is associated with its own tropopause undulation as can be discerned by routine inspection of vertical cross sections of wind speed and potential vorticity (PV). The Arctic jet is less ubiquitous but is confined to high latitudes and is often located at about 500 hPa (Shapiro et al. 1984; Shapiro 1985; Shapiro et al. 1987).

Corresponding author: Jonathan E. Martin, jemarti1@wisc.edu

DOI: 10.1175/JCLI-D-16-0565.1

Careful observational work by Defant and Taba (1957, hereinafter DT57) established the existence of a three-step structure in tropopause height from pole to equator with each step separated from its neighbors by the presence of a westerly wind maximum. The tropical tropopause was found (in the mean) to be at about 90 hPa (17–18 km) and to extend to about 30°N. Near that latitude, the tropopause height abruptly lowers to about 200 hPa. The subtropical jet is coincident with this break in tropopause height and is located at about 200 hPa (12 km). Poleward of this feature was what DT57 called the ''middle tropopause'' located at about 250 hPa. At the break between this middle tropopause and the even lower polar tropopause is the polar jet, located at about 300 hPa. Modest, shallow baroclinicity in the upper troposphere characterizes the subtropical jet, whereas the much deeper and more dramatically baroclinic polar front drapes below the polar jet.

A new insight represented by the DT57 analysis was their construction of maps of tropopause height (in hPa). They referred to sharp, isolated, easily identifiable gradients of tropopause height as ''breaklines'' (see their Fig. 2). These breaklines were found to be coincident with the axes of the respective jet maxima (e.g., the subtropical jet was located at the breakline between the tropical and middle tropopause).[1] Such depictions made it instantly clear that, though each jet maximum occupied a climatological latitude band, substantial meanders of each were commonplace. Companion maps of tropopause temperature presented by DT57 clearly demonstrated that when the polar and subtropical jets become latitudinally superposed the tropospheric and stratospheric baroclinicity associated with each jet individually were combined into substantially narrower zones of contrast. The resulting superposed jet structure therefore possessed an anomalous fraction of the pole-to-equator baroclinicity [manifest as available potential energy (APE)].

An alternative method for identifying the tropopause breaklines of DT57 lies in the construction of tropopause maps in potential temperature–potential vorticity (θ–PV) space. Such an approach was advocated by Morgan and Nielsen-Gammon (1998), who demonstrated the utility of maps of θ and wind speed on the so-called dynamic tropopause [defined as a surface of constant Ertel PV (Ertel 1942)] for diagnosing weather systems. In this framework, the DT57 breaklines become regions of large PV gradient on isentropes that cut through the subtropical and polar jet cores since such isentropes sample both stratospheric and tropospheric air.

By virtue of their enhanced wind speeds and baroclinicity, superposed jets are characterized by invigorated horizontal and vertical circulations (Handlos and Martin 2016) and have been connected, either directly or indirectly, with a number of previously examined high-impact, midlatitude sensible weather phenomena. Defant (1959) noted that an exceptional surface cyclogenesis event south of Iceland on 8 January 1956, in which the sea level pressure (SLP) dropped 61 hPa in 20 h, developed in an environment characterized by a dramatic jet superposition event. Other famous explosive cyclogenesis events such as the Great October Storm (Hoskins and Berrisford 1988), the Experiment on Rapidly Intensifying Cyclones over the Atlantic (ERICA) IOP-4 storm (Shapiro and Keyser 1990), the Cleveland Superbomb (Hakim et al. 1996), and the Storm of the Century (Bosart et al. 1996) are all examples of developments likely influenced by a jet superposition event.[2]

More recently, Winters and Martin (2014, 2016) examined the influence the secondary circulations associated with superposed jet structures had in forcing a rapid increase in poleward moisture flux that fueled the second day of the 2010 Nashville Flood and in the development of a major winter storm in the northeastern United States. In addition, the 25–28 April 2011 severe weather outbreak across the central and eastern portion of North America (Christenson and Martin 2012; Knupp et al. 2014) has been linked to a superposed jet structure that formed over the western Pacific Ocean.

Superposition events also exhibit ties to elements of the Northern Hemisphere large-scale circulation. In their examination of the large-scale environments conducive to jet superposition in the western Pacific, Handlos and Martin (2016) showed that these events are by-products of the surge phase of the East Asian winter monsoon (EAWM). Additionally, Handlos (2016) has shown that such events lead to zonal extension of the jet, a leading mode of Pacific jet variability (Eichelberger and Hartmann 2007; Athanasiadis et al. 2010; Jaffe et al. 2011; Griffin and Martin 2016).

Despite the appearance of jet superposition events as a fundamental ingredient in a number of high-impact, midlatitude weather environments, and their association with large-scale circulation phenomena during the cold season [November–March (NDJFM)], there is neither

[1] Equation (1) (to be discussed later) demonstrates that local maxima in the geostrophic wind $\mathbf{V}_g$ are coincident with large horizontal gradients of QGPV.

[2] At some point in their respective evolutions, all of these cases were characterized by a two-step tropopause structure similar to that portrayed in Fig. 1d.

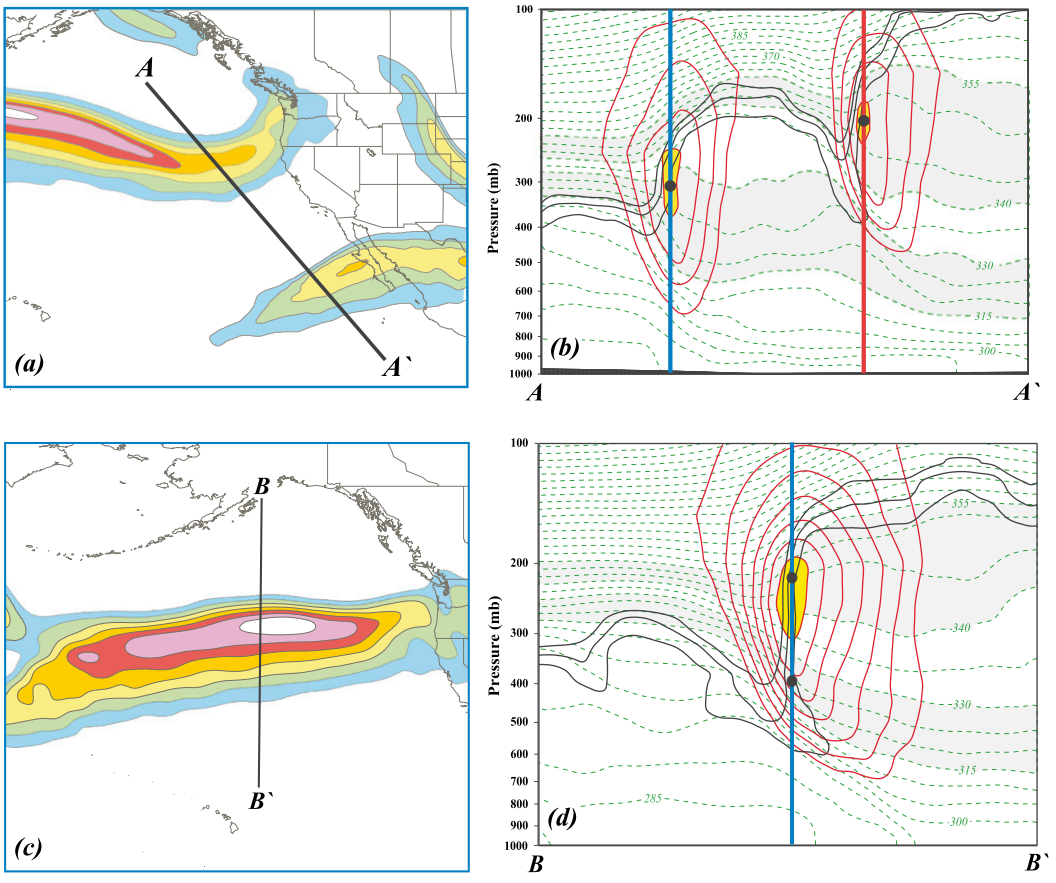

FIG. 1. (a) The 300-hPa isotachs (shaded every 10 m s $^{-1}$, starting at 30 m s^{-1}) at 0000 UTC 27 April 2010 depicting separate polar and subtropical jets. (b) Cross section along A–A′ in (a). Solid black lines are isertels of 1–3 PVU. Dashed lines are isentropes contoured every 5 K. Red solid lines are isotachs (m s^{-1}) and contoured every 10 m s^{-1}, starting at 30 m s^{-1}. The jet cores are shaded yellow and the 315–330- and 340–355-K isentropic layers are shaded gray. The blue (red) line corresponds to a grid column in which the black dot confirms a polar (subtropical) jet identification. (c) As in (a), but at 0000 UTC 24 October 2010. (d) As in (b), but along the cross section B–B′ in (c). The blue line corresponds to a grid column in which a jet superposition (i.e., a polar and subtropical jet in the same column) is identified.

synoptic climatology of these features nor any systematic observational study of the mechanism(s) by which the polar and subtropical jets become vertically superposed. It is the goal of this paper to provide a cold season synoptic climatology of Northern Hemisphere jet superpositions.

The paper is organized as follows. Section 2 provides a description of the datasets and methodology used to objectively identify the polar jet, subtropical jet, and locations where the two are vertically superposed. Section 3 presents the results of a 50-yr, cold season synoptic climatology of the frequency and distribution of each species of tropopause-level jet. The climatology of jet superposition events is presented in section 4. Finally, section 5 discusses the results in the context of other studies of jet stream climatology and offers final comments and conclusions, along with suggestions for future work.

2. Data and methodology

Considered from a PV perspective, the subtropical and polar jets are each associated with local positive PV perturbations at the equatorward edge of the tropopause. Most often, the separate jet cores, as well as the separate PV perturbations, are readily identifiable as illustrated in Figs. 1a,b. Note that the PV distribution displayed in Fig. 1b portrays the three-step tropopause structure identified by DT57. Note also that the separate polar and subtropical jet cores, though widely separated in latitude and elevation, are each found at a ''break'' in dynamic tropopause height represented by a locally

steep tropopause slope. A superposed jet structure cannot be identified solely by inspection of the distribution of isotachs on an isobaric surface (Fig. 1c). Instead, the distinguishing structural characteristic of such features is the vertical tropopause wall directly connecting the tropical tropopause to the polar tropopause (Fig. 1d). The development of such a structure has dynamical implications that are most simply considered from the quasigeostrophic PV (QGPV) perspective. Recall that QGPV is given by

$$q_g = \frac{1}{f_o}\nabla^2\phi + f + \frac{\partial}{\partial p}\left(\frac{f_o}{\sigma}\frac{\partial\phi}{\partial p}\right) = \Lambda(\phi) + f,$$

where $\Lambda = f_o^{-1}\nabla^2 + \partial/\partial p(f_o/\sigma)\partial/\partial p + (f_o/\sigma)\partial^2/\partial p^2$, and ϕ is the geopotential. The cross-jet gradient of QGPV $\partial q_g/\partial n$, where $\hat{n}$ is the cross-flow direction in natural coordinates, is then given by

$$\frac{\partial q_g}{\partial n} = \Lambda\left(\frac{\partial\phi}{\partial n}\right) = \Lambda(-fV_g), \tag{1}$$

after substituting from the natural coordinate expression for the geostrophic wind (Cunningham and Keyser 2004). The deep tropopause wall arises via an increase in $\partial q_g/\partial n$ through a deep layer {i.e., $-\partial/\partial p[\partial/\partial t(\partial q_g/\partial n)] > 0$}.

A central analysis question thus becomes, which isentropic layers most frequently house the separate polar and subtropical jets? Various prior studies (e.g., DT57; Palmén and Newton 1969; Shapiro et al. 1987; Morgan and Nielsen-Gammon 1998; Mecikalski and Tripoli 1998; Shapiro et al. 1999; Randel et al. 2007) have suggested a fairly narrow range of acceptable values; 310–320 K for the polar jet and 335–345 K for the subtropical jet. In the present work, the choice is made via two rather distinct analyses of 50 yr of NCEP reanalysis data (1960/61–2009/10).

The first method begins by interpolating the data into 5-K isentropic layers spanning from 300–305 to 375–380 K. The interpolated data are then employed to calculate PV in each layer. Since the jets are tied to the low-PV edge of the strong PV gradient at the tropopause, the magnitude of the zonally averaged PV gradient between the 1- and 3-PVU (1 PVU = 10^{-6} K kg^{-1} m^2 s^{-1}) isertels in each layer for each day is calculated in the following manner. In each layer, the area A enclosed by the 1-PVU isertel is calculated and then converted to an equivalent latitude ϕ_e by the formula

$$\phi_e = \arcsin\left(1 - \frac{A}{2\pi R_e^2}\right),$$

where R_e is the radius of Earth. After applying the same procedure to the 3-PVU isertel, the meridional distance between the two equivalent latitudes Δy is an inverse measure of the intensity of the zonally averaged 1–3-PVU gradient in that layer on that day. Daily averages of Δy in each layer over the 50 seasons are calculated next. To further smooth the data, we calculate the cold season average of these daily average values. The resulting 1 November–31 March average Δy in each layer is plotted in Fig. 2a. The analysis reveals two minima in Δy (maxima in $|\nabla_h \mathrm{PV}|$) and that they occupy the 315–330- and 340–355-K isentropic layers.

In support of the foregoing analysis, we also considered the isentropic level at which the maximum wind speed was observed in each grid column (between 10° and 80°N) at each analysis time in the 50-yr time series. Note that only grid columns in which the integral average wind speed exceeded 30 m s^{-1} within the 100–400-hPa layer[3] were considered in the census. The results of this analysis indicate a clear bimodal distribution with twin frequency maxima in the 310–325- and 340–355-K layers (Fig. 2b). The combined analyses in Fig. 2 compel adoption of the 315–330- and 340–355-K layers as the respective isentropic space residences of the polar and subtropical jets.

The climatology is constructed from 50 cold seasons (NDJFM) of National Centers for Environmental Prediction (NCEP)–National Center for Atmospheric Research (NCAR) reanalysis data, at 6-h intervals, spanning the period 1 November 1960–31 March 2010. The NCEP–NCAR reanalysis data are available at 17 isobaric levels (1000, 925, 850, 700, 600, 500, 400, 300, 250, 200, 150, 100, 70, 50, 30, 20, and 10 hPa) with a 2.5° latitude–longitude grid spacing (Kalnay et al. 1996; Kistler et al. 2001).[4] These data were bilinearly interpolated onto isentropic surfaces at 5-K intervals from 300 to 370 K using programs within the General Meteorology Package (GEMPAK) (desJardins et al. 1991).

To identify the polar, subtropical, and superposed jet streams an automated, objective identification scheme was developed whose criteria can be described with reference to the features illustrated in Fig. 1 and the analysis described in the prior section. Figure 1a clearly portrays two distinct jets located off the west coast of North America with the polar jet feature near the Oregon–Washington border and the subtropical jet zonally oriented over Mexico. A vertical cross section taken through the polar and subtropical jet cores (Fig. 1b) shows that the polar jet, located at approximately 300 hPa, is largely contained within

[3] Following Koch et al. (2006), the integral average wind speed is found by using $\mathrm{AVG} = 1/(p_2 - p_1)\int_{p_1}^{p_2}(u^2 + v^2)^{1/2}\,\partial p$.

[4] The sensitivity of the results to grid spacing was tested by employing the higher-resolution (0.5° × 0.5° grid spacing) NCEP Climate System Forecast Reanalysis (CFSR) data (Saha et al. 2010) over 32 cold seasons (1979–2010). The results were quite similar to those obtained using the NCEP–NCAR reanalysis data.

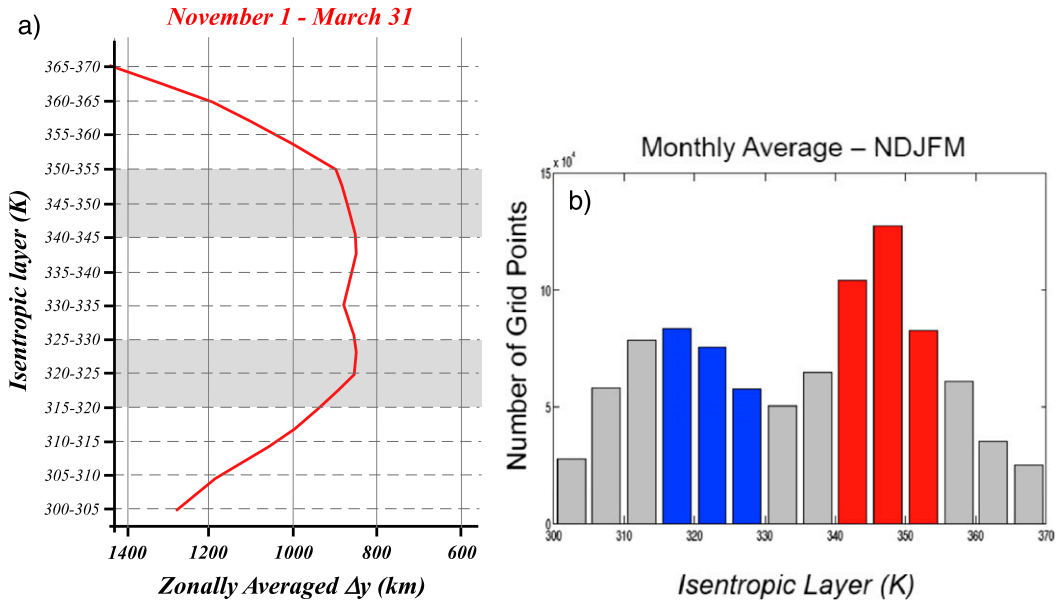

FIG. 2. (a) Cold season average of zonally averaged Δy (km) for 5-K isentropic layers ranging from 300–305 to 365–370 K. The 315–330- and 340–355-K layers are highlighted in light gray shading. (b) The average frequency of occurrence of grid points with a maximum wind speed value within the 5-K isentropic layers along the abscissa per cold season. The 315–330- and 340–355-K layers are shaded in blue and red, respectively.

the 315–330-K isentropic layer, while the subtropical jet core, located at approximately 200 hPa, occupies the 340–355-K layer. Additionally, both the polar and the subtropical jets lie at the low-PV edge of the strong horizontal PV gradient that separates the upper troposphere from the lower stratosphere within each respective isentropic layer. The isertels are locally quite steep in the vicinity of the jet cores. In fact, considering the 2-PVU contour as the dynamic tropopause, it is clear that the tropopause breaklines of DT57, which portrayed the steep slope of the tropopause near the jet axes, are exactly equivalent to regions of large $|\nabla_h \mathrm{PV}|$ in the 1–3-PVU channel, which represents the boundary between the stratosphere and troposphere. Given these basic structural elements, the identification scheme evaluates characteristics of the PV and wind speed distributions in each grid column. Within the 315–330-K (340–355 K) layer, whenever the magnitude of the PV gradient within the 1–3-PVU channel exceeds an empirically determined threshold value[5] and the integral average wind speed in the 400–100-hPa layer exceeds 30 m s^{-1}, we identify a polar (subtropical) jet in that grid column.

Occasionally, the two jets superpose in the vertical, creating a hybrid of both the subtropical and polar jets characterized by a single isotach maximum, as illustrated in Fig. 1c. A vertical cross section taken through the jet core, as shown in Fig. 1d, thus illustrates that the criteria for both the polar and subtropical jet are identified in a single vertical grid column, identifying a superposed jet. Notice that, rather than the three-step tropopause structure identified by DT57 and shown in Fig. 1b, a superposed jet is characterized by a two-step tropopause structure with a steep tropopause break from the polar to the tropical tropopause. This nearly vertical PV wall (from ~550 to ~150 hPa in this case) is a leading structural characteristic of these features. It is important to note that since the scheme does not consider the lateral, cross-flow width of the jet species, it does not identify superpositions in instances in which, for example, the northern edge of a bundle of subtropical jet isotachs might overlap the southern edge of a polar jet bundle. Such instances do not exhibit the characteristic vertical PV wall.

The identification scheme is applied to each 6-h analysis time in the 50 cold seasons to objectively identify grid point locations of the subtropical jet, polar jet, and jet superposition events. The total number of possible identifications for each grid point in each month of a given year is equal to 4 times the number of days in

[5] The threshold value is 0.64×10^{-5} PVU m^{-1} (0.64×10^{-11} m K kg^{-1} s^{-1}) for both the 315–330- and 340–350-K layers. This value was determined by extensive analysis of vertical cross sections through jets in order to determine the minimum value of $|\nabla_h \mathrm{PV}|$ required to reliably identify the deep tropopause wall characteristic of superposed jets. For each isentropic layer, the threshold value exceeds the 50th percentile for $|\nabla_h \mathrm{PV}|$ in grid columns located in the 1–3-PVU channel with integrated wind speed exceeding 30 m s^{-1}.

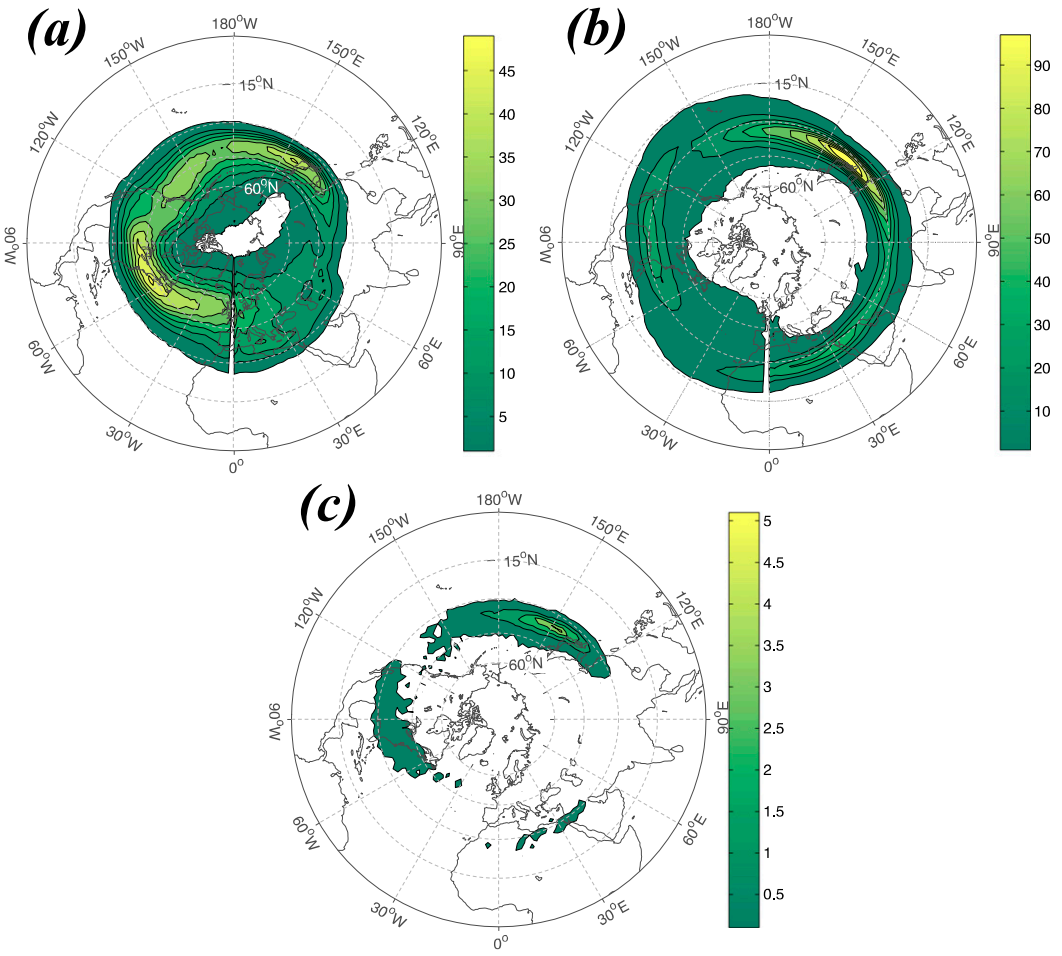

FIG. 3. Average frequency of occurrence per cold season (NDJFM) of Northern Hemisphere (a) polar jet, (b) subtropical jet, and (c) superposed jet IDs constructed from the 50 cold seasons in the interval 1960/61–2009/10. Note the frequency scale is different for each panel.

the month.[6] The identifications are then compiled to reveal the spatial and temporal distribution of all three tropopause-level jet species. In addition, the speed and direction of the wind at 250 hPa is recorded for each grid column in which a jet superposition is identified.

3. Analysis of jet distributions

In this section the results of the objective identification (ID) of the polar and subtropical jet species are presented as frequency distributions in both seasonal and monthly form. The analysis begins by considering the frequency distributions for the polar jet.

a. Polar jet

During the Northern Hemisphere cold season (NDJFM), the polar jet is found most frequently over the eastern portions of North America and the northern portions of the Atlantic Ocean (Fig. 3a). In the Pacific basin the polar jet is distributed rather uniformly with localized maxima located south of Alaska and near Japan. Notably, the polar jet is far less frequent over the Eastern Hemisphere than over the Western Hemisphere. Partitioning the cold season into its constituent months reveals a number of interesting subseasonal characteristics in the frequency and distribution of the polar jet.

The November frequency distribution (Fig. 4a) is characterized by separate maxima near Japan and south of Alaska. The axis of maximum polar jet frequency over the Atlantic sector stretches from central North America to the British Isles. In December narrow

[6] For example, for a given grid point, each January, with 31 days in the month, would have 124 possible identifications.

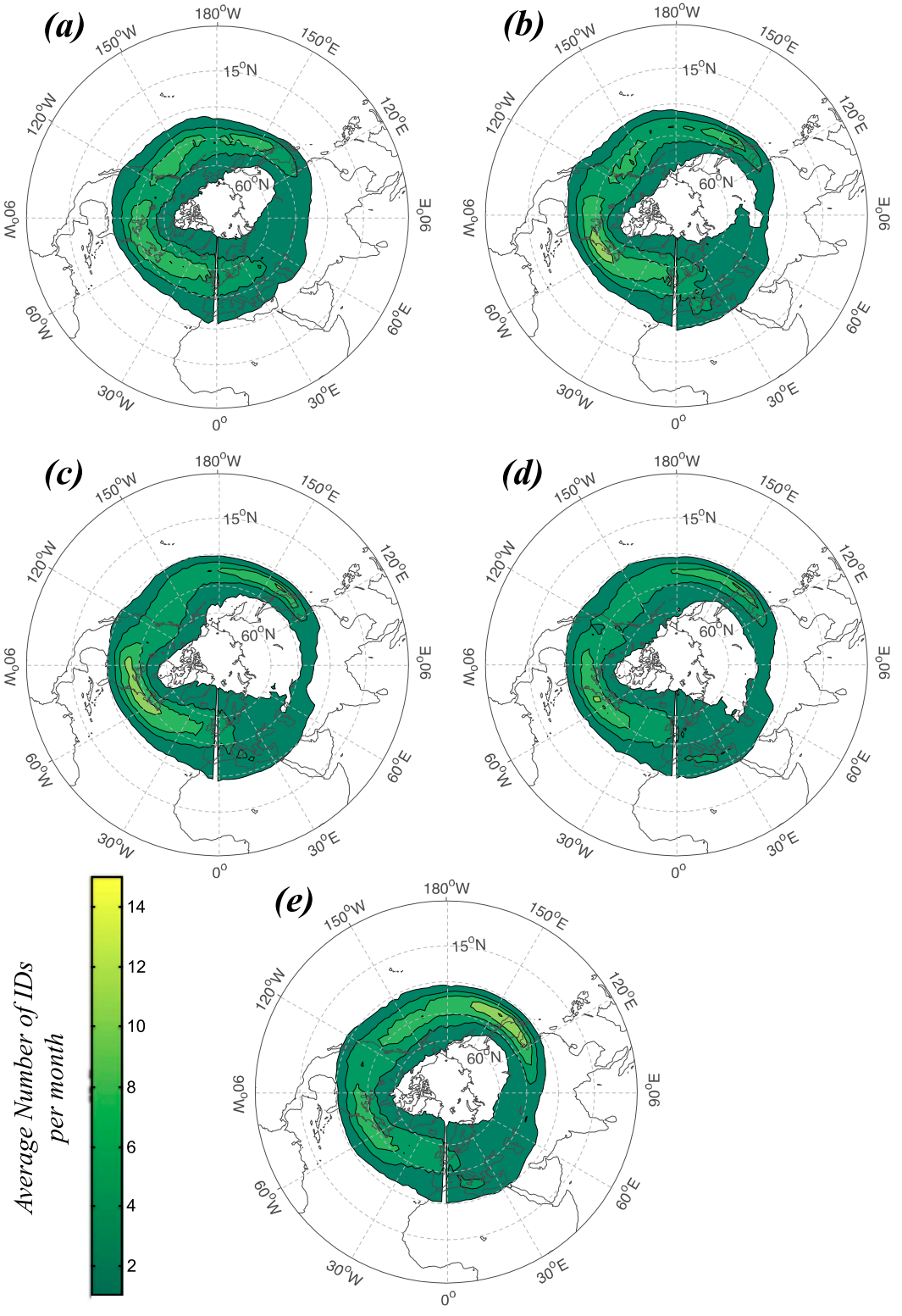

FIG. 4. Monthly average frequency of occurrence of Northern Hemisphere polar jet IDs for the months of (a) November, (b) December, (c) January, (d) February, and (e) March.

latitude bands of maximum frequency exist in the western portions of both ocean basins (Fig. 4b). These bands broaden across the basin from west to east indicating greater variability of the flow in the eastern portions of both basins. Also worthy of note is the fact that the axis of greatest frequency in both basins shifts dramatically equatorward from November to December.

January has a similar frequency distribution as December with a continued but less dramatic shift equatorward in both basins (Fig. 4c). Interestingly, the polar jet remains much more common in the Atlantic than in the Pacific basin, although the western Pacific basin frequency maxima continues to narrow and extend zonally. By February, the Atlantic (Pacific) frequency maxima has decreased (increased) slightly with the only other notable change being a decrease in polar jet frequency extending from the west coast of North America to the south central Great Plains of the United States (Fig. 4d).

A dramatic shift in the hemispheric frequency maxima from the Atlantic to the Pacific (Fig. 4e) characterizes the distribution in March. The frequency maxima in the Pacific (Atlantic) basin also increase (decrease) during March. While barely noticeable in Fig. 4e, the polar jet shifts 2.5° latitude northward during March in the western Pacific basin as it begins its poleward migration north for the summer.

b. *Subtropical jet*

During the Northern Hemisphere cold season the subtropical jet has a frequency maximum in the western Pacific over Japan that extends westward to southern China and eastward to the date line (Fig. 3b). This local maximum is embedded within an axis of maximum frequency that stretches across the entire Eastern Hemisphere at approximately 30°N. The central Pacific and southern North America, along with northwest Africa, are other regions with frequent subtropical jet activity during the cold season.

In November the subtropical jet frequency maximum in the Pacific, previously spread over a wide latitude band in the western Pacific basin (not shown) is consolidated into a narrow latitudinal strip centered on Japan (Fig. 5a). The wide band of low-frequency distribution over North America and the North Atlantic testifies to the variability of the subtropical jet location in these regions during November. By December, the axis of maximum subtropical jet frequency has expanded both eastward and westward but remains fixed near 32.5°N, while the maximum in frequency has increased to greater than 25 times per month in some locations (Fig. 5b). January represents the month of maximum subtropical jet frequency with a large swath of greater than 31 identifications per month across northern Japan (Fig. 5c). January is also the first month that exhibits a thin band of greater than 7 identifications per month stretching westward from the southern portion of Asia to North Africa. February has nearly the same hemispheric distribution as January but with a small reduction in the western Pacific frequency maximum (Fig. 5d). Throughout the winter months, the subtropical jet frequency maximum shifts westward (Figs. 5b–d). The distribution in March is quite similar to the distributions in the preceding winter months albeit with reduced frequencies (Fig. 5e).

4. Jet superpositions

As described previously, a jet superposition (alternatively, a superposed jet) occurs when both the polar jet and subtropical jet are identified in the same vertical grid column. In this section the frequency distribution of such structures is presented.

a. *Distribution of jet superpositions*

The cold season distribution of jet superpositions is clearly maximized in the western Pacific basin just east of Japan (Fig. 3c). A secondary frequency maximum stretches across southern North America out to the southern maritime provinces of Canada. The third very weak local frequency maximum is evident over the southeastern Mediterranean Sea. Monthly frequency distributions, again, provide a refined perspective on the characteristic cold season circulation evolution.

November superposition events occur across the entire Pacific basin with a slight frequency maximum east of Japan (Fig. 6a). A separate axis of frequency maximum stretches from the central United States toward the North Atlantic (Fig. 6a). By December, the robust local maximum in jet superposition events in the western Pacific first presents itself (Fig. 6b). This dramatic increase results from an increased frequency, as well as a decreased variability, of both the subtropical and polar jets in this region at this time of year. In fact, in December the axis of maximum frequency of the two jet species are typically separated by only a few degrees of latitude in the western Pacific. The western Pacific frequency maximum reaches its annual peak just east of Japan in January (Fig. 6c).This increased frequency appears related to an increased frequency of the subtropical jet. Despite a coherent increase in the polar jet frequency, the frequency of jet superpositions in the western Pacific decreases in February (Fig. 6d). In fact, despite the frequency and close proximity of the polar and subtropical jets during western Pacific winter,

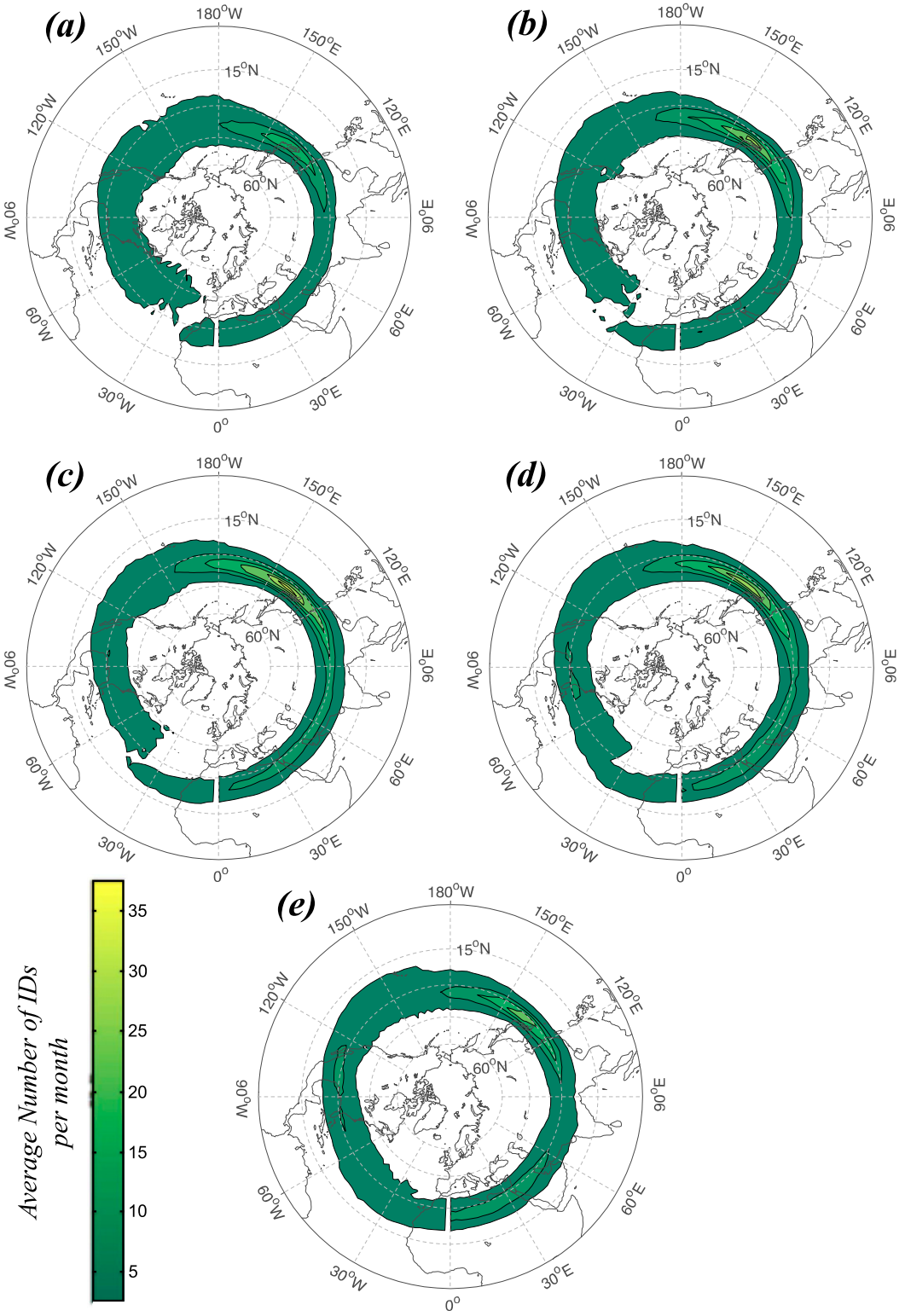

FIG. 5. As in Fig. 4, but for Northern Hemisphere subtropical jet IDs.

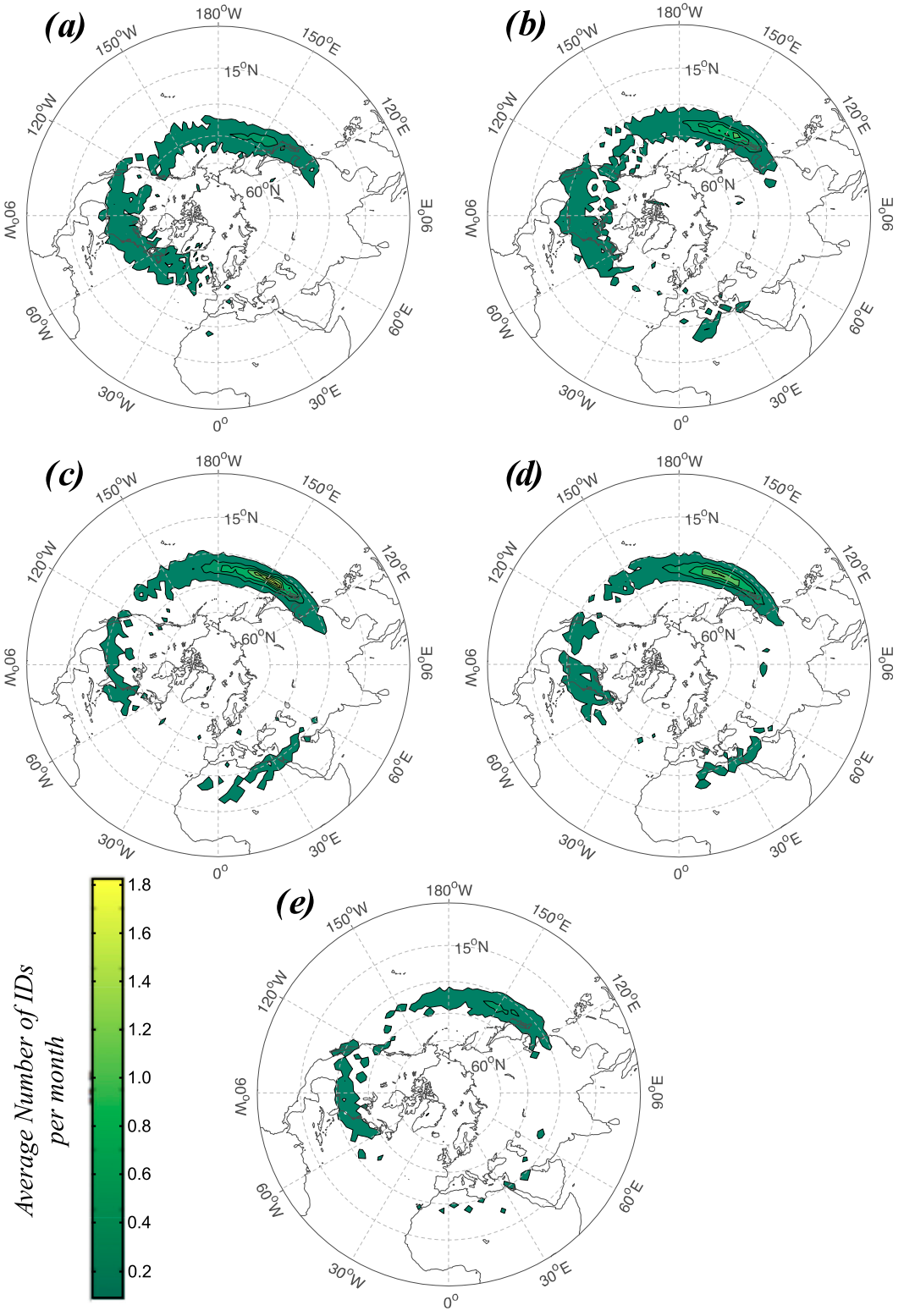

FIG. 6. As in Fig. 4, but for Northern Hemisphere superposed jet IDs.

evident through a comparison of Figs. 4b–d and Figs. 5b–d, vertical superposition of the two species remains a rare event. Despite the annual maximum in Pacific basin polar jet frequency that characterizes March (Fig. 4e), the number of jet superpositions significantly decreases there in the same month (Fig. 6e). This decrease in frequency is likely tied to the corresponding decrease in the subtropical jet frequency (Fig. 4e).

b. *Additional characteristics of superposed jets*

To further characterize the nature of superposed jets, for each event identified in the 50-season climatology we examined the wind direction and speed at 250 hPa. The average 250-hPa wind speed associated with all superpositions observed during November is 77.0 m s^{-1} while the wind direction is solidly west-southwest (WSW) (Fig. 7a). December has nearly as many WSW as west jet superpositions, which are accompanied by an increase in the average wind speed to 83.5 m s^{-1} (Fig. 7b). The primary wind direction for January jet superpositions veers back to westerly as over half of the superpositions in January are associated with a west wind (Fig. 7c). The average wind speed also continues to increase reaching 90.1 m s^{-1} by this time. These observations make clear that superposed jets are some of the strongest jets found in the hemisphere. The speed and direction characteristics of February are nearly identical to January's with over half of superpositions associated with a westerly wind, while the average wind speed increases fractionally to 90.3 m s^{-1} (Fig. 7d). As spring approaches in the Northern Hemisphere, the average wind speed of jet superpositions decreases to 83.0 m s^{-1} in March (Fig. 7e). The wind direction also begins to back as WSW is, once again, established as the most frequent wind direction.

The unusual strength of superposed jets is further illustrated in Fig. 8, which shows the monthly distribution of the average maximum wind speeds found in columns identified as containing polar, subtropical, or superposed jets. It is clear that superposed jets are characteristically associated with much stronger wind speeds than either the polar or subtropical jets. This observation is consistent with the presumption that the secondary circulation associated with such jets is also more vigorous as noted in several recent observational studies (Christenson and Martin 2012; Winters and Martin 2014, 2016, 2017; Handlos and Martin 2016).

c. *Comparison to NDJFM mean zonal wind*

The Northern Hemisphere tropopause-level flow is often considered from the perspective of the mean zonal wind at some upper-tropospheric isobaric level. Though this perspective is analytically simple, it fails to account for the more complicated distribution of the polar and subtropical jets revealed by the preceding analysis. Figure 9 illustrates aspects of the obfuscation engendered by this popular approach. The wintertime polar jet frequency maxima lie on the poleward edge of the 250-hPa seasonal mean zonal wind around the entire hemisphere (Fig. 9a). In addition, the portions of the eastern Pacific and North Atlantic where the 250-hPa mean zonal wind fails to reach 30 m s^{-1} and yet the polar jet is found with regularity suggests that the polar jet is highly variable in those regions. The subtropical jet frequency maxima, on the other hand, are found in the core of the average zonal wind isotachs from North Africa eastward to the central Pacific (Fig. 9b) suggesting a prominent role for the subtropical jet in the annual tropopause-level wind climatology over this vast area. Over North America, however, the subtropical jet is found on the equatorward edge of the average 250-hPa zonal wind, suggesting that the average zonal wind in this region is nearly equally composed of polar jet and subtropical jet components. The jet superposition frequency maximum in the Pacific is displaced eastward and slightly poleward of the zonal wind maximum there. Whether this distribution suggests that superposition events in the western Pacific preferentially result from equatorward excursions of the polar jet at the entrance to the Pacific storm track is a subject for future inquiry. Similarly intriguing is the fact that the superposition maximum in the Atlantic is nearly coincident with the local zonal wind maximum (Fig. 9c).

5. Summary and discussion

Jet streams or jets, defined as narrow, rapidly flowing currents of air located near the tropopause, often play a significant role in sensible weather in the midlatitudes. Two species of jets have been identified in prior studies, the polar (or eddy-driven) jet and the subtropical jet. Some of the most significant findings regarding the large-scale distribution of Northern Hemisphere jet streams were advanced by DT57, when they first published horizontal maps of tropopause heights. Since its introduction in 1957, the only amendment to DT57's conception of a three-step tropopause structure came from Shapiro et al. (1987), who suggested the addition of the Arctic-jet and Arctic-tropopause step.

Though somewhat infrequently, the polar and subtropical jets occasionally become vertically superposed. Aside from scattered mentions in studies by Mohri (1953), Riehl (1962), Reiter (1961, 1963), and Reiter and Whitney (1969), such phenomena have only recently enjoyed renewed consideration (e.g., Winters and

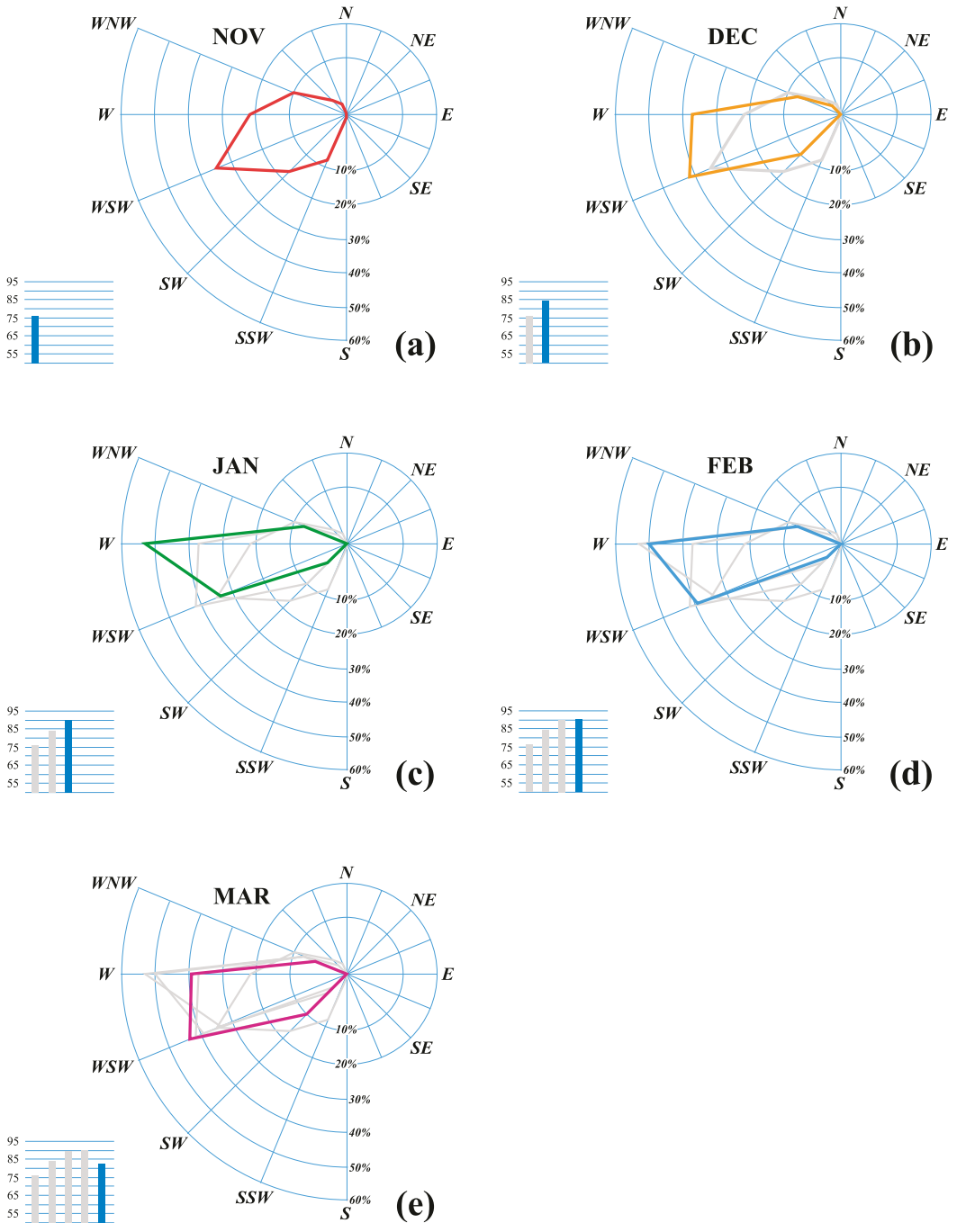

FIG. 7. (a) Wind direction plotted on the wind rose for every Northern Hemisphere jet superposition identified during the 50 Novembers in the analysis. Average wind speed ($m\,s^{-1}$) for each jet superposition shown in blue on the bar graph. (b) As in (a), but for December. The thin gray line on the wind rose and gray bar graph represents prior month's direction and speed data. (c) As in (b), but for January. (d) As in (b), but for February. (e) As for (b), but for March.

Martin 2014, 2016, 2017; Handlos and Martin 2016). Motivated by the connections between jet superposition, significant weather events and large-scale circulation phenomena such as the EAWM, the present study has employed an objective jet stream identification scheme to construct a 50-yr cold season climatology of Northern Hemisphere polar, subtropical, and superposed jets. The analysis demonstrates that cold season

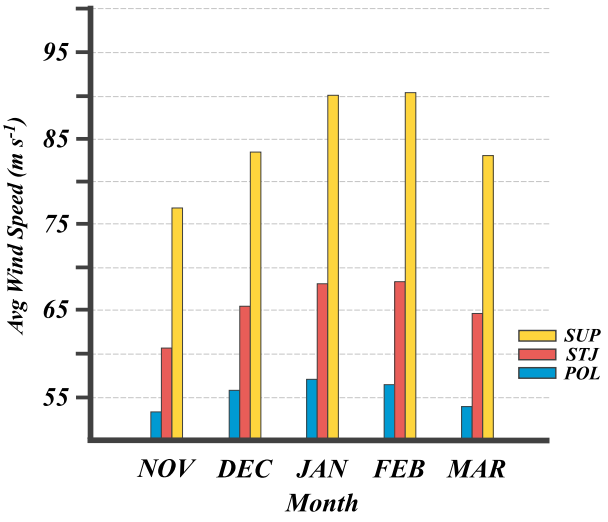

FIG. 8. Average maximum wind speed in columns identified as polar (POL; light blue), subtropical (STJ; red), or superposed (SUP; yellow) jets for each month in the 50-yr cold season time series.

jet superposition events occur most often in the western Pacific near Japan, with other regional maxima residing over the southern United States–North Atlantic and North Africa (Fig. 3c). Superposition events occur most (less) often during DJF (November–March). In the western Pacific (North Atlantic), a maximum in the frequency of occurrence of the subtropical (polar) jet exists on average during the cold season. It is important to note that, despite the regional maximum in superposition frequency along with the close proximity of the polar (Fig. 4) and subtropical jets (Fig. 5) in the western Pacific, jet superpositions are still relatively rare occurrences.

In their examination of the distribution of Northern Hemisphere jet streams, Koch et al. (2006) used an integrated-wind-speed threshold to identify the jet streams. They further subdivided their jet identification into two subcategories; those jet features with shallow baroclinicity were classified as subtropical jets while those with deep baroclinicity were classified as polar jets. Broadly speaking, the results of their shallow baroclinicity classification correlate well with the findings presented in our work (their Fig. 6 compared to our Fig. 3b). When the deep baroclinicity classification is compared, however, significant differences exist (their Fig. 7 and our Fig. 3a). First, their winter maximum in the deep baroclinicity (polar) jet in the Atlantic is less expansive than the Atlantic polar jet frequency maximum reported in the present analysis. Second, the Pacific basin is significantly different, with two maxima present in the Koch et al. (2006) analysis, while a single latitude band maximum is present in our analysis (Fig. 3a). Unfortunately, the Koch et al. (2006) classification scheme is not amenable to the identification of jet superposition events. The identification scheme introduced in this paper, which takes into account an integrated wind speed as well as a PV-gradient threshold within specified tropopause-crossing isentropic layers, allows each jet type to be identified separately and so also allows identification of jet superpositions.

The idealized modeling results of Lee and Kim (2003) suggested that a strong and poleward-directed subtropical jet coincides with a more equatorward polar (eddy driven) jet while a weaker, more zonal subtropical jet tends to be accompanied by increased poleward displacement of the polar jet. They further suggested that the western Pacific sector corresponds to a strong subtropical jet (STJ) regime while the Atlantic sector most often displays a weak STJ. Given the above associations, it is perhaps unsurprising that the frequency maximum of jet superpositions revealed by the present analysis occurs in the western Pacific basin (Fig. 3b).

The analysis and methodology presented in this paper provide a framework for objective identification of the tropopause-level polar and subtropical jets. Identification of the polar jet using near-surface or lower-tropospheric winds is a popular approach (e.g., Lorenz and Hartmann 2003; Hartmann 2007; Woollings et al. 2010; Barnes and Polvani 2013) that is consistent with its midlatitude, eddy-driven origins. Despite the physical insights garnered by such studies, the eddy-driven jet perspective perhaps deemphasizes consideration of the tropopause break identified by DT57 as a characteristic of the polar jet. Geostrophic cold air advection along the polar jet axis often results in differential tilting across that tropopause break and a downward extrusion of stratospheric PV into the upper troposphere above 700 hPa (Shapiro 1981; Keyser and Pecnick 1985; Martin 2014), leading to the production of midtropospheric features that are ultimately responsible for the development of surface cyclones. Interest in such important structural and dynamical characteristics of polar jet life cycles motivates the alternative tropopause-based identification approach presented here.

Winters and Martin (2016) examined the synoptic and mesoscale processes supporting jet superposition in two contrasting cases over the eastern United States. They found that ageostrophic transverse circulations associated with the jet circulations themselves were instrumental in producing a downward protrusion of high-PV air between the two originally separate jet cores. In combination with latent heat release and irrotational flow associated with convection, this subsidence

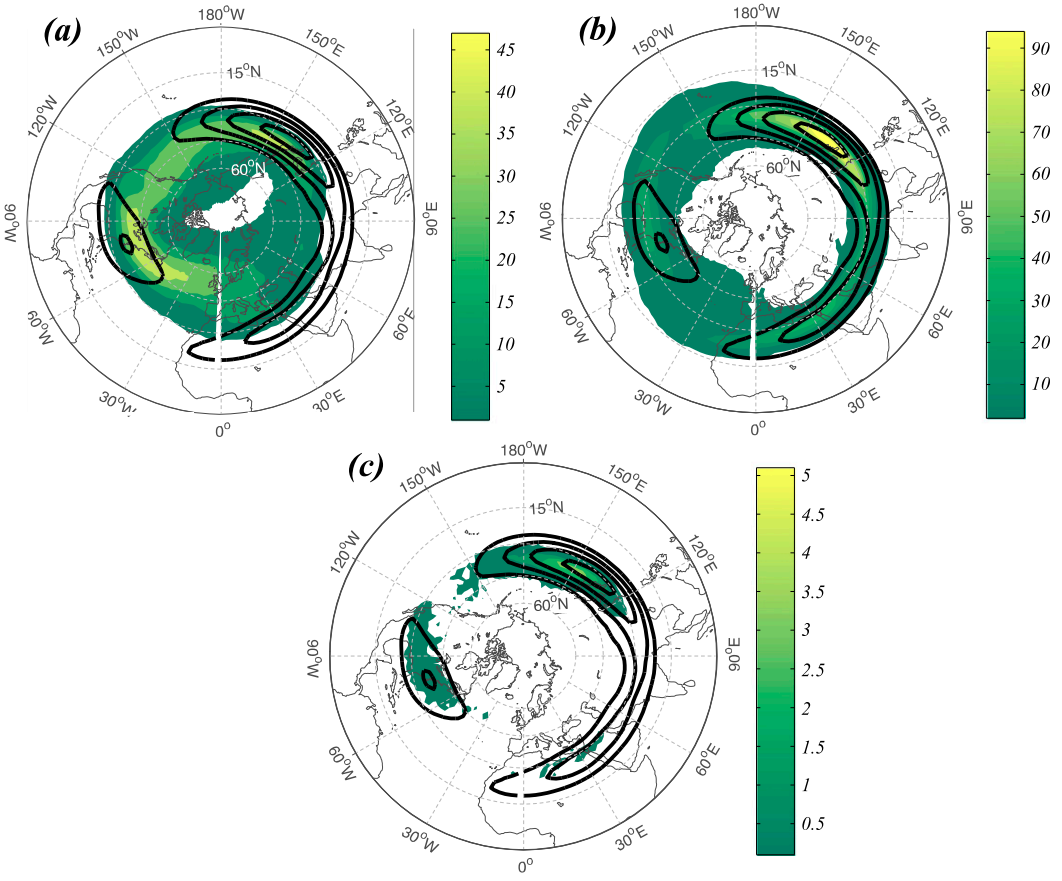

FIG. 9. As in Fig. 3, but with the cold season climatological 250-hPa zonal wind plotted every 10 m s^{-1}, starting at 30 m s^{-1}, in thick black solid contour.

contributed to the production of the steep tropopause wall characteristic of the superposed jet environment. A novel isentropic partitioning of the perturbation PV was employed by Winters and Martin (2017) to perform a piecewise PV inversion of the tropopause disturbances associated with the separate polar and subtropical jets. They found that the 3D circulation associated with the polar jet PV (the nondivergent wind associated with the subtropical jet PV) controlled the vertical (horizontal) restructuring of the tropopause associated with building the steep tropopause PV wall that attended the jet superposition in their case.

The work presented in this study motivates a number of additional research questions. One such question regards the frequency distributions of the polar, subtropical, and superposed jets in the Southern Hemisphere. Additionally, application of the Winters and Martin (2017) analysis tools to selected cases in the western Pacific region is currently under way. Given that the polar and subtropical jets are frequently in very close proximity to one another there during the winter [as first suggested by Riehl (1962)], we hope to better understand why vertical superposition there is nonetheless so rare.

Additional future work, with implications for understanding changes in the general circulation in a warmer climate, will apply our identification scheme to the output from selected CMIP5 simulations. As the evidence for Arctic amplification increases and the pole-to-equator temperature gradient relaxes in the lower troposphere, it is plausible that a warmer planet will be characterized by a hemispheric reduction of the polar jet. However, given the moist neutrality of the tropical atmosphere, any warming of the surface will be reflected by larger warming aloft. Therefore it is not inconceivable that a warmer planet will feature enhanced baroclinicity in the tropical–subtropical upper troposphere–lower stratosphere (UTLS), thus supporting a stronger subtropical jet.

Finally, the interaction between, and superposition of, the polar and subtropical jets—which has served as the focus of this paper—represents perhaps one of the most conspicuous and synoptic-scale manifestations of tropical–extratropical interaction. To the extent that the

frequency and distribution of these features, along with the synoptic and mesoscale dynamics associated with them, are better understood, so will be the diagnoses and prognoses of weather systems in both the current and future climate.

Acknowledgments. This work was funded by the National Science Foundation through Grant AGS-1265182. We thank three anonymous reviewers for helpful comments that improved the manuscript.

REFERENCES

Athanasiadis, P. J., J. M. Wallace, and J. J. Wettstein, 2010: Patterns of wintertime jet stream variability and their relation to the storm tracks. *J. Atmos. Sci.*, **67**, 1361–1381, doi:10.1175/2009JAS3270.1.

Barnes, E. A., and L. Polvani, 2013: Response of the midlatitude jets, and of their variability, to increased greenhouse gases in the CMIP5 models. *J. Climate*, **26**, 7117–7135, doi:10.1175/JCLI-D-12-00536.1.

Bosart, L. F., G. J. Hakim, K. R. Tyle, M. A. Bedrick, W. E. Bracken, M. J. Dickinson, and D. M. Schultz, 1996: Large-scale antecedent conditions associated with the 12–14 March 1993 cyclone ("Superstorm '93") over eastern North America. *Mon. Wea. Rev.*, **124**, 1865–1891, doi:10.1175/1520-0493(1996)124<1865:LSACAW>2.0.CO;2.

Christenson, C. E., and J. E. Martin, 2012: The large-scale environment associated with the 25–28 April 2011 severe weather outbreak. *16th Annual Severe Storms and Doppler Radar Conf.*, Des Moines, IA, National Weather Association.

Cunningham, P., and D. Keyser, 2004: Dynamics of jet streaks in a stratified quasi-geostrophic atmosphere: Steady-state representations. *Quart. J. Roy. Meteor. Soc.*, **130**, 1579–1609, doi:10.1256/qj.03.35.

Defant, F., 1959: On hydrodynamic instability caused by an approach of subtropical and polarfront jet stream in northern latitudes before the onset of strong cyclogenesis. *The Atmosphere and Sea in Motion*, B. Bolin, Ed., Rockefeller Institute Press, 305–325.

——, and H. Taba, 1957: The threefold structure of the atmosphere and the characteristics of the tropopause. *Tellus*, **9**, 259–275, doi:10.3402/tellusa.v9i3.9112.

desJardins, M. L., K. F. Brill, and S. S. Schotz, 1991: Use of GEMPAK on UNIX workstations. *7th Int. Conf. on Interactive Information and Processing Systems for Meteorology, Oceanography, and Hydrology*, New Orleans, LA, Amer. Meteor. Soc., 449–453.

Eichelberger, S. J., and D. L. Hartmann, 2007: Zonal jet structure and the leading mode of variability. *J. Climate*, **20**, 5149–5163, doi:10.1175/JCLI4279.1.

Ertel, H., 1942: Ein neuer hydrodynamischer Wirbelsatz. *Meteor. Z.*, **59**, 277–281.

Griffin, K. S., and J. E. Martin, 2016: Synoptic features associated with temporally coherent modes of variability of the North Pacific jet stream. *J. Climate*, **30**, 39–54, doi:10.1175/JCLI-D-15-0833.1.

Hakim, G. J., D. Keyser, and L. F. Bosart, 1996: The Ohio valley wave merger cyclogenesis event of 25–26 January 1978. Part II: Diagnosis using quasigeostrophic potential vorticity inversion. *Mon. Wea. Rev.*, **124**, 2176–2205, doi:10.1175/1520-0493(1996)124<2176:TOVWMC>2.0.CO;2.

Handlos, Z. J., 2016: Composite and case study analyses of the large-scale environments associated with west Pacific polar and subtropical vertical jet superposition events. Ph.D. dissertation, Dept. of Atmospheric and Oceanic Sciences, University of Wisconsin–Madison, 168 pp.

——, and J. E. Martin, 2016: Composite analysis of large-scale environments conducive to west Pacific polar/subtropical jet superposition. *J. Climate*, **29**, 7145–7165, doi:10.1175/JCLI-D-16-0044.1.

Hartmann, D. L., 2007: The general circulation of the atmosphere and its variability. *J. Meteor. Soc. Japan*, **85B**, 123–143, doi:10.2151/jmsj.85B.123.

Held, I. M., 1975: Momentum transport by quasi-geostrophic eddies. *J. Atmos. Sci.*, **32**, 1494–1497, doi:10.1175/1520-0469(1975)032<1494:MTBQGE>2.0.CO;2.

Hoskins, B. J., and P. Berrisford, 1988: A potential vorticity perspective of the storm of 15–16 October 1987. *Weather*, **43**, 122–129, doi:10.1002/j.1477-8696.1988.tb03890.x.

Jaffe, S. C., J. E. Martin, D. J. Vimont, and D. J. Lorenz, 2011: A synoptic climatology of episodic, subseasonal retractions of the Pacific jet. *J. Climate*, **24**, 2846–2860, doi:10.1175/2010JCLI3995.1.

Kalnay, E., and Coauthors, 1996: The NCEP/NCAR 40-Year Reanalysis Project. *Bull. Amer. Meteor. Soc.*, **77**, 437–470, doi:10.1175/1520-0477(1996)077<0437:TNYRP>2.0.CO;2.

Keyser, D., and M. J. Pecnick, 1985: A two-dimensional primitive equation model of frontogenesis forced by confluence and horizontal shear. *J. Atmos. Sci.*, **42**, 1259–1282, doi:10.1175/1520-0469(1985)042<1259:ATDPEM>2.0.CO;2.

——, and M. A. Shapiro, 1986: A review of the structure and dynamics of upper-level frontal zones. *Mon. Wea. Rev.*, **114**, 452–499, doi:10.1175/1520-0493(1986)114<0452:AROTSA>2.0.CO;2.

Kistler, R., and Coauthors, 2001: The NCEP–NCAR 50-Year Reanalysis: Monthly means CD-ROM and documentation. *Bull. Amer. Meteor. Soc.*, **82**, 247–267, doi:10.1175/1520-0477(2001)082<0247:TNNYRM>2.3.CO;2.

Knupp, K. R., and Coauthors, 2014: Meteorological overview of the devastating 27 April 2011 tornado outbreak. *Bull. Amer. Meteor. Soc.*, **95**, 1041–1062, doi:10.1175/BAMS-D-11-00229.1.

Koch, P., H. Wernli, and H. C. Davies, 2006: An event-based jet-stream climatology and typology. *Int. J. Climatol.*, **26**, 283–301, doi:10.1002/joc.1255.

Koteswaram, P., 1953: An analysis of the high tropospheric wind circulation over India in winter. *Indian J. Meteor. Geophys.*, **4**, 13–21.

——, and S. Parthasarathy, 1954: The mean jet stream over India in the pre-monsoon and post-monsoon seasons and vertical motions associated with subtropical jet streams. *Indian J. Meteor. Geophys.*, **5**, 138–156.

Krishnamurti, T. N., 1961: The subtropical jet stream of winter. *J. Meteor.*, **18**, 172–191, doi:10.1175/1520-0469(1961)018<0172:TSJSOW>2.0.CO;2.

Lee, S., and H.-K. Kim, 2003: The dynamical relationship between subtropical and eddy-driven jets. *J. Atmos. Sci.*, **60**, 1490–1503, doi:10.1175/1520-0469(2003)060<1490:TDRBSA>2.0.CO;2.

Loewe, F., and V. Radok, 1950: A meridional aerological cross section in the southwest Pacific. *J. Meteor.*, **7**, 58–65.

Lorenz, D. J., and D. L. Hartmann, 2003: Eddy–zonal flow feedback in the Northern Hemisphere winter. *J. Climate*, **16**, 1212–1227, doi:10.1175/1520-0442(2003)16<1212:EFFITN>2.0.CO;2.

Martin, J. E., 2014: Quasi-geostrophic diagnosis of the influence of vorticity advection on the development of upper level jet-front

systems. *Quart. J. Roy. Meteor. Soc.*, **140**, 2658–2671, doi:10.1002/qj.2333.

McWilliams, J. C., and J. H. S. Chow, 1981: Equilibrium geostrophic turbulence I: Reference solution in a β-plane channel. *J. Phys. Oceanogr.*, **11**, 921–949, doi:10.1175/1520-0485(1981)011<0921:EGTIAR>2.0.CO;2.

Mecikalski, J. R., and G. J. Tripoli, 1998: Inertial available kinetic energy and the dynamics of tropical plume formation. *Mon. Wea. Rev.*, **126**, 2200–2216, doi:10.1175/1520-0493(1998)126<2200:IAKEAT>2.0.CO;2.

Mohri, K., 1953: On the fields of wind and temperature over Japan and adjacent waters during winter of 1950-1951. *Tellus*, **5A**, 340–358, doi:10.3402/tellusa.v5i3.8582.

Morgan, M. C., and J. W. Nielsen-Gammon, 1998: Using tropopause maps to diagnose midlatitude weather systems. *Mon. Wea. Rev.*, **126**, 2555–2579, doi:10.1175/1520-0493(1998)126<2555:UTMTDM>2.0.CO;2.

Namias, J., and P. F. Clapp, 1949: Confluence theory of the high tropospheric jet stream. *J. Meteor.*, **6**, 330–336, doi:10.1175/1520-0469(1949)006<0330:CTOTHT>2.0.CO;2.

Newton, C. W., 1954: Frontogenesis and frontolysis as a three-dimensional process. *J. Meteor.*, **11**, 449–461, doi:10.1175/1520-0469(1954)011<0449:FAFAAT>2.0.CO;2.

Palmén, E., and C. W. Newton, 1969: *Atmospheric Circulation Systems: Their Structure and Physical Interpretation*. Academic Press, 603 pp.

Panetta, R. L., 1993: Zonal jets in wide baroclinically unstable regions: Persistence and scale selection. *J. Atmos. Sci.*, **50**, 2073–2106, doi:10.1175/1520-0469(1993)050<2073:ZJIWBU>2.0.CO;2.

Randel, W. J., D. J. Seidel, and L. L. Pan, 2007: Observational characteristics of double tropopauses. *J. Geophys. Res.*, **112**, D07309, doi:10.1029/2006JD007904.

Reiter, E. R., 1961: *Meteorologie der Strahlströme*. Springer-Verlag, 473 pp.

——, 1963: *Jet Stream Meteorology*. University of Chicago Press, 515 pp.

——, and L. F. Whitney, 1969: Interaction between subtropical and polar-front jet stream. *Mon. Wea. Rev.*, **97**, 432–438, doi:10.1175/1520-0493(1969)097<0432:IBSAPJ>2.3.CO;2.

Rhines, P. B., 1975: Waves and turbulence on a beta-plane. *J. Fluid Mech.*, **69**, 417–433, doi:10.1017/S0022112075001504.

Riehl, H., 1962: Jet streams of the atmosphere. Colorado State University Dept. of Atmospheric Science Tech. Rep. 32, 117 pp.

Saha, S., and Coauthors, 2010: The NCEP Climate Forecast System Reanalysis. *Bull. Amer. Meteor. Soc.*, **91**, 1015–1057, doi:10.1175/2010BAMS3001.1.

Shapiro, M. A., 1981: Frontogenesis and geostrophically forced secondary circulations in the vicinity of jet stream-frontal zone systems. *J. Atmos. Sci.*, **38**, 954–973, doi:10.1175/1520-0469(1981)038<0954:FAGFSC>2.0.CO;2.

——, 1985: Dropwindsonde observations of an Icelandic low and a Greenland mountain-lee wave. *Mon. Wea. Rev.*, **113**, 680–683, doi:10.1175/1520-0493(1985)113<0680:DOOAIL>2.0.CO;2.

——, and D. Keyser, 1990: Fronts, jet streams and the tropopause. *Extratropical Cyclones: The Erik Palmen Memorial Volume*, C. Newton and E. O. Holopainen, Eds., Amer. Meteor. Soc., 167–191.

——, R. C. Schnell, F. P. Parungo, S. J. Oltmans, and B. A. Bodhaine, 1984: El Chichón volcanic debris in an Arctic tropopause fold. *Geophys. Res. Lett.*, **11**, 421–424, doi:10.1029/GL011i005p00421.

——, T. Hampel, and A. J. Krueger, 1987: The Arctic tropopause fold. *Mon. Wea. Rev.*, **115**, 444–454, doi:10.1175/1520-0493(1987)115<0444:TATF>2.0.CO;2.

——, and Coauthors, 1999: A planetary-scale to mesoscale perspective of the life cycles of extratropical cyclones: The bridge between theory and observations. *The Life Cycle of Extratropical Cyclones*, M. A. Shapiro and S. Gronas, Eds., Amer. Meteor. Soc., 139–185.

Sutcliffe, R. C., and J. K. Bannon, 1954: Seasonal changes in the upper-air conditions in the Mediterranean–Middle East area. *Proc. Int. Association of Meteorology (UGGI)*, Rome, Italy, UGGI, 322–334.

Winters, A. C., and J. E. Martin, 2014: The role of a polar/subtropical jet superposition in the May 2010 Nashville Flood. *Wea. Forecasting*, **29**, 954–974, doi:10.1175/WAF-D-13-00124.1.

——, and ——, 2016: Synoptic and mesoscale processes supporting vertical superposition of the polar and subtropical jets in two contrasting cases. *Quart. J. Roy. Meteor. Soc.*, **142**, 1133–1149, doi:10.1002/qj.2718.

——, and ——, 2017: Diagnosis of a North American polar/subtropical jet superposition employing potential vorticity inversion. *Mon. Wea. Rev.*, **145**, 1853–1873, doi:10.1175/MWR-D-16-0262.1.

Woollings, T., A. Hannachi, and B. Hoskins, 2010: Variability of the North Atlantic eddy-driven jet stream. *Quart. J. Roy. Meteor. Soc.*, **136**, 856–868, doi:10.1002/qj.625.

Yeh, T. C., 1950: The circulation of the high troposphere over China in the winter of 1945–46. *Tellus*, **2A**, 173–183, doi:10.3402/tellusa.v2i3.8548.